Exp Fluids (2009) 46:65–76
DOI 10.1007/s00348-008-0539-8

RESEARCH ARTICLE

Unsteady flow diagnostics using weak perturbations

Beric Skews · Harald Kleine

Received: 22 April 2008 / Revised: 2 July 2008 / Accepted: 3 July 2008 / Published online: 27 July 2008

Abstract The examination of the motion of very weak waves generated from small sources on the boundary of a flow domain gives information on how the domain shape influences the flow, both from spatial and temporal perspectives. In the study of shock wave dynamics the shock itself generates a weak wave when passing over a small step, or surface irregularity. The basic principle is that if a particle produces a series of point disturbances in a flow field, the induced perturbations will propagate outwards at the local sonic velocity whilst at the same time being convected along with the local flow velocity. A number of issues may be identified for an unsteady flow. Firstly, the flow field at later times may be influenced by perturbations produced at earlier times. Secondly, if the positions of the perturbations can be monitored as a function of time, then the trajectory and velocity of the particle may be deduced. Thirdly, if a perturbation arises from a point on a boundary, then its influence, if any, on any particular part of the flow can be established. A number of examples are presented to illustrate the value of the technique and its potential to uncover the mechanisms responsible for the formation of certain flow patterns in high-speed compressible flows.

B. Skews (✉)
School of Mechanical, Industrial, and Aeronautical Engineering,
University of the Witwatersrand, PO Wits,
Johannesburg 2050, South Africa
e-mail: beric.skews@wits.ac.za

H. Kleine
School of Aerospace, Civil, and Mechanical Engineering,
University of New South Wales,
Australian Defence Force Academy, Canberra,
ACT 2600, Australia

1 Introduction

The technique of placing small transverse perturbation sources, such as strips of tape, on the wall of a supersonic wind tunnel to evaluate the flow uniformity and to determine the Mach number from the measurement of the Mach angle in a steady flow is well known. An extension of this approach is shown in the steady flow of Fig. 1, where very shallow triangular grooves are machined on the surface of the body. The Mach number distribution on the surface of the body may then be estimated from measurement of the local Mach angle at any point as long as the flow remains supersonic. In the shown example, the blunt nose of the body leads to a detached bow shock and thus a subsonic zone embedded in the supersonic flow. The extent of this zone becomes visible on the image. Although it is not a very accurate measurement, an estimate of the point where the sonic line meets the surface can be made on the basis of the pattern seen in Fig. 1. The transition from sub- to supersonic flow close to the surface occurs where the angle of the perturbation, or Mach line, at the wall becomes perpendicular to it.

The same idea may be extended to unsteady flows. The nature of the perturbed flow field induced by a particle moving in a straight line in a compressible medium is a standard textbook illustration of the distinction between subsonic, sonic, and supersonic flow. Here, the particle is the disturbance source. However, the idea applies equally well to a particle moving along an arbitrary path at variable velocity as illustrated by Lilley and Yates (1953) for the case of a particle moving at non-uniform velocity along a straight path. Consider, for example, a particle, starting from rest, accelerating along a curved path to supersonic velocity as shown in Fig. 2.

Each disturbance pulse generated by the particle will propagate outwards at sonic velocity in all directions with

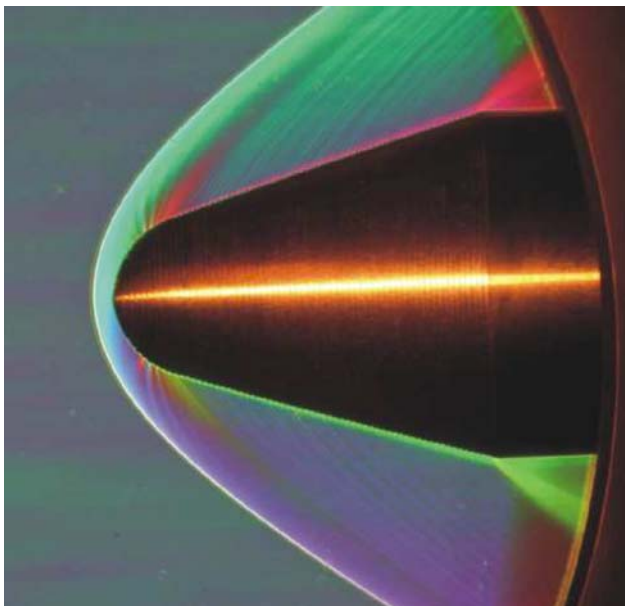

Fig. 1 Supersonic flow ($M = 2.4$) around a blunt axisymmetric body showing Mach lines emanating from the surface due to surface perturbation sources

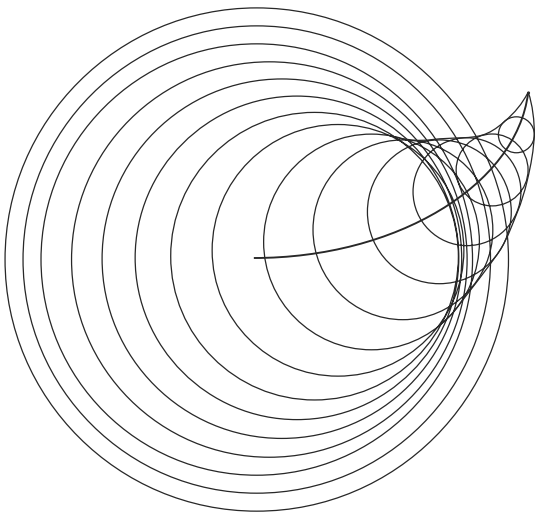

Fig. 2 Perturbation field for a particle starting from rest and accelerating to supersonic velocity along a curved trajectory

the centre of its circle of influence at the position where the pulse was emitted. As the particle moves, a series of waves is produced. This illustrates a number of issues. Firstly, the flow field at later times is influenced by perturbations produced at earlier times even if the particle is moving at supersonic velocity. Secondly, if the positions of the perturbations can be monitored as a function of time, then the trajectory and velocity of the particle may be deduced. Thirdly, if a perturbation arises from a point on a boundary, then its influence, if any, on any particular part of the flow can be established. This is shown to be important in the current study for the propagation and focussing of shock waves from a curved surface. The illustration of Fig. 2 is for the ideal case where the perturbation fronts remain circular, and local expansion and compression regions, as well as shear, do not distort them.

2 Shock wave induced perturbations

When a plane shock wave moves down a constant area duct and passes over a minute wall imperfection, a weak perturbation will propagate out into the following flow as indicated in Fig. 3, which shows the flow field at a time t after the shock has passed over the perturbation source. The flow behind the shock is uniform in velocity and sound speed and thus the propagating disturbance will remain circular with a radius at, where a is the post-shock sound speed. In the same time, the shock will move a distance Vt, and the perturbation centre a distance ut from the source, where V and u are the shock and post-shock gas velocity, respectively. Both the velocity and sound speed behind the shock may be calculated from well-known relations for moving shock waves. The position where the perturbation strikes the shock will be specified by the angle m as shown in Fig. 3. Above this point the incident shock has no

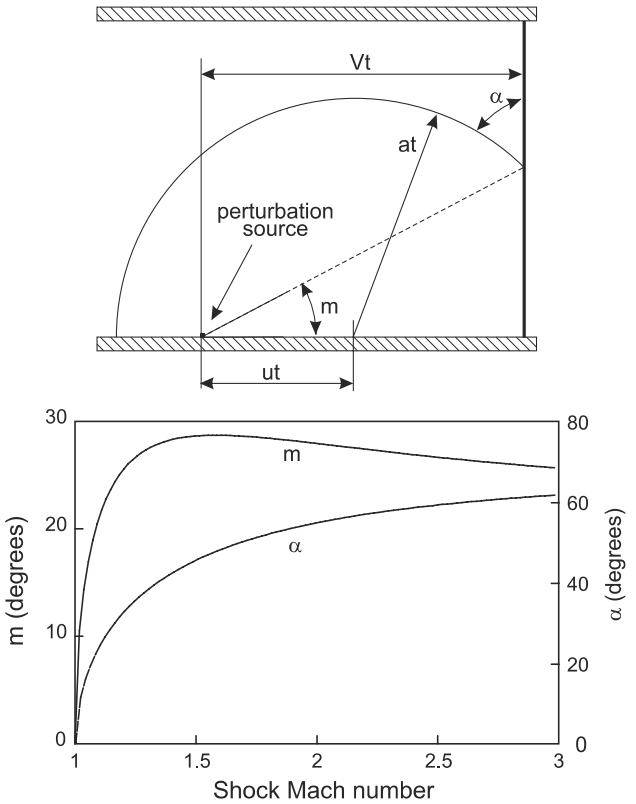

Fig. 3 Acoustic perturbation resulting from a shock wave passing over a small wall imperfection

knowledge of the existence of the wall imperfection since no information radiating out has reached it. The value of m as a function of the shock wave Mach number M_s has previously been derived (Skews 1967) and is given by:

$$\tan^2 m = (\gamma - 1)(M_s - 1)\{M_s^2 + 2/(\gamma - 1)\}/(\gamma + 1)M_s^4 \quad (1)$$

where γ is the specific heats ratio. The angle α between the perturbation signal where it meets the shock and the incident shock may also simply be established from the geometry.

$$\cos \alpha = M_s a_0/a - M \quad (2)$$

where a_0 is the sound speed ahead of the shock and M is the Mach number of the flow induced by the moving shock.

It is noted that the angles m and α are very sensitive to Mach number for weak shocks, and their measurement could even be used as a basis for determining the shock velocity. The angle m is analogous to the angle of the characteristics in Whitham's well-known shock dynamics formulation (Whitham 1967), but as shown in (Skews 1967), there are substantial differences in their magnitudes for shocks with shock Mach numbers below $M_s = 2$. One of the earliest examples of using a weak wave for flow diagnostics in a shock tube was done by Lock and Dewey (1989).

3 Open-cell foams

When a plane shock wave impacts on an open cell foam slab, a complex interaction takes place including both a reflected wave back into the gas and a transmitted wave into the foam. Of interest here are the visible features of the reflection. Figure 4 shows a pair of schlieren photographs

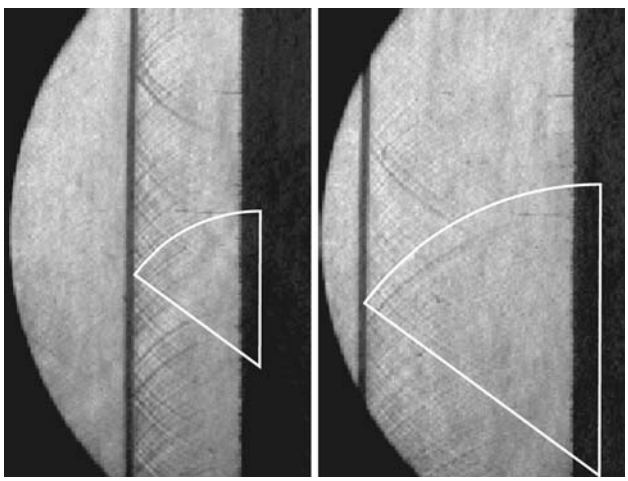

Fig. 4 Two stages of reflected wave development following shock wave impact on an porous foam block

taken 100 μs apart with the reflected wave propagating to the left. These clearly show a myriad of waves propagating out from the pores as the flow enters the slab and multiple reflections from within the pore structure, which build up to form the reflected shock. In this case the pores are randomly distributed and the source for any particular wave cannot be established. There is, however, a clearly defined structure to the wavelets consisting of clear circular patterns, being more defined closer to the shock which arose from the earlier part of the interaction, and more diffuse closer to the foam face as the path for waves to emerge becomes more tortuous. However, some useful information may still be derived. Firstly it is noted that fitting a circular arc to the perturbations shows its centre lying behind the foam face. This indicates that the source of the perturbation on impact has convected through the foam face into the foam and this gives a measure of the gas inflow. Taking the ratio of distance of penetration into the foam to the distance the reflected shock has moved away, the inflow appears to decrease in time. This is consistent with pressure measurement data which shows that flows into the face of the foam eventually ceases due to collapse of the pores causing the foam to become impermeable (Seitz and Skews 2006). Secondly, considering a frame of reference fixed in the gas ahead of the foam, an estimate may be made of the angle α between the shock front and the wavelet, as defined in Fig. 3. This will give the relative reflected shock Mach number and is found to correlate reasonably well with measurements taken of arrival times of the reflected shock measured by side-wall pressure transducers, knowing the incident shock Mach number. Furthermore, since the time interval between the two images is known, the increase in the radius of the circular arc enables an estimate to be made of the sound speed behind the reflected wave. Images with more clearly defined perturbations would be beneficial for such quantitative analysis to be useful. A slightly stronger wavelet arriving from the top and bottom of the specimen and propagating towards the centre is noted. This is the corner signal generated at the moment of impact generated at the corner between the specimen and the upper and lower shock tube walls. In this case the origin of the perturbation is known and a single image would suffice to obtain quantitative information.

Similar analyses can be done for shock impact on an inclined foam surface as shown in Fig. 5. Although the perturbations are very weak, some estimate of the inflow may be made for wavelets generated at different times as the shock propagated over the surface. Of particular importance is the distinct thickening of the reflected shock wave as the wavelets coalesce to form a compression wave, indicating a dispersed nature of the reflected wave as the compression waves from within the foam emerge through its surface. Unfortunately such tests become less useful at

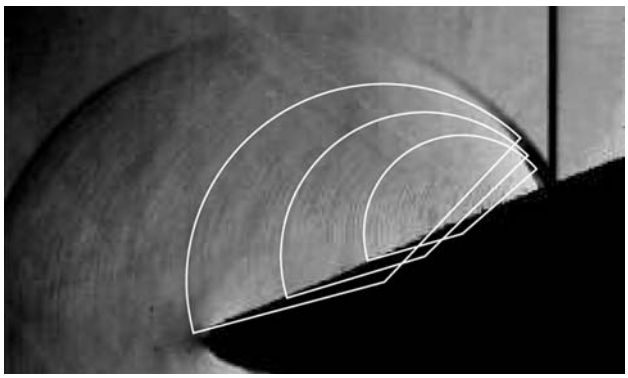

Fig. 5 Gas penetration following shock wave impingement on a foam wedge

longer times due to the transverse collapse of the specimen arising from the foam dragging on the walls once it starts moving.

4 Grid perturbations

In a similar fashion to the procedure described above, useful information can be obtained for shock wave impact on a rigid grid. Three examples are given in Fig. 6. The top shadowgraph is for oblique impact on a 20% blockage grid, with an incident shock Mach number of 1.36. Blockage is defined as the ratio of the overall area closed to flow to the total area. Thus 100% blockage is an impermeable surface, and 0% represents no restriction to the flow. The lower pair of images are interferograms of tests with a grid of 67% blockage. The upper one shows Mach reflection and the lower a regular reflection. In both cases the black fringes, which are lines of constant density, take on a zig-zag pattern, shown at double magnification in the small images to the right, as they pass through the perturbed region. This gives an indication of the weakness of the perturbed waves arising from the surface as each reflected compression wavelet arising from the solid part of the surface is followed by an expansion as the shock passes through a slit. The fact that they are weak makes them amenable to the analysis as suggested in Sect. 2, and done in (Skews and Takayama 1996). In the two regular reflection cases the flow velocity in the perturbed region behind the reflection point is supersonic in a frame of reference fixed in the reflection point. Thus information from the bottom corner inlet of the model cannot propagate into this region. The separation between the pseudo-steady flow near the reflection point and the unsteady flow around the inlet corner is identified by the so-called corner signal, C, as shown, and by the change of the reflected shock from being plane to it being curved.

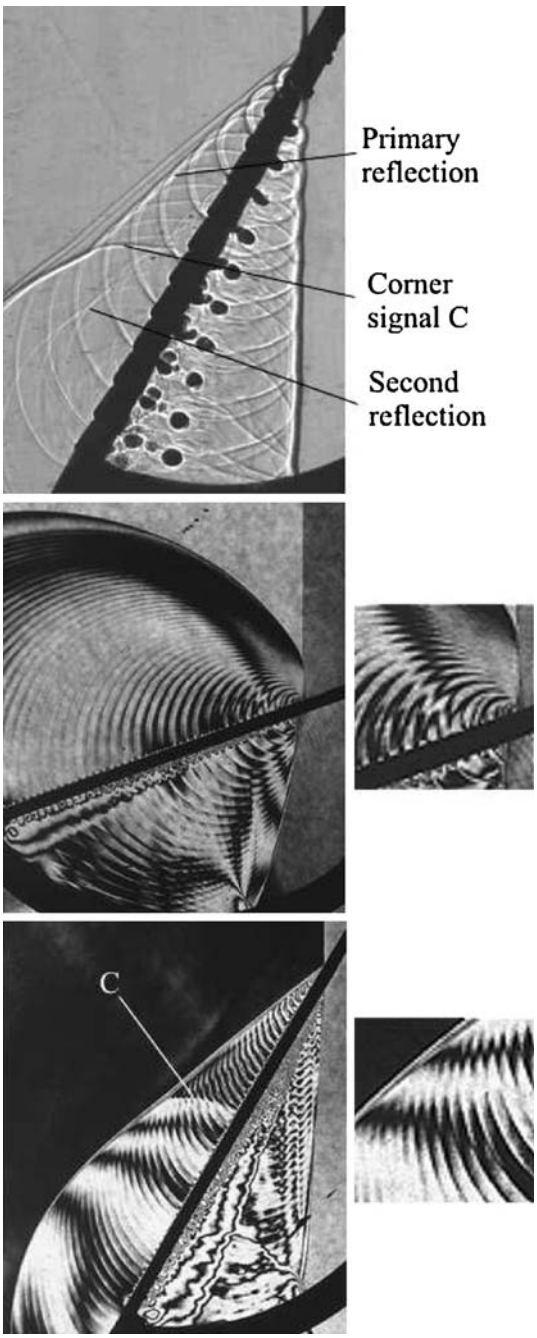

Fig. 6 Images of shock wave interactions with an inclined grid. *Top* Shadowgraph (Skews 2005). *Lower pair* Interferograms (Courtesy: K. Takayama, Tohoku University). C is the corner signal

In the pseudo-steady region the inflow into the wall may simply be obtained by applying the oblique shock equations across the incident and reflected shocks, from knowing the incident shock strength and the angles the waves make with the grid surface. An alternative suggestion is to assume that the perturbations in the vicinity of the wall are circular and that determining their centres will, as in the foam case dealt with above, give a measure of the

inflow. Both these methods have been used (Skews and Takayama 1996) with the result shown in Fig. 7. The centre of the circular perturbation is convected from S to A as the shock reflection point moves from S to D, and the inflow angle β is measured relative to where the wavelet intersects the grid. For a stationary observer the inflow angle relative to the plate is ε. The two methods agree satisfactorily when the reflection is regular and the flow is pseudo-steady, but they deviate markedly during Mach reflection. The perturbation analysis will be more valid in the unsteady region than two-shock or three-shock analysis which assumes plane waves and uniform flow fields. This is because the perturbations propagate into a non-uniform region depending on the local state of the gas and therefore reflect its properties without any assumptions been made about its uniformity. Applying the pseudo-steady assumption is clearly suspect within the diffraction field induced by the curved portion of the reflected wave. This analysis indicates diminishing inflow as the wall angle decreases, but still shows finite inflow at glancing incidence.

An interesting feature is noted in the shadowgraph image of Fig. 6 in that a second faint reflected wave is visible between the main reflected wave and the grid surface. This is caused by wavelet re-reflection from the bottom of the slits, and could be used to determine how the inflow adjusts to the guidance through the slits. Similar analyses can be done for the transmitted wave although care has to be taken in distinguishing between the waves generated at the upper and lower surface of each slit. However, since the shed vortices under the plate move at particle velocity tracking them is more useful in determining the gas velocity.

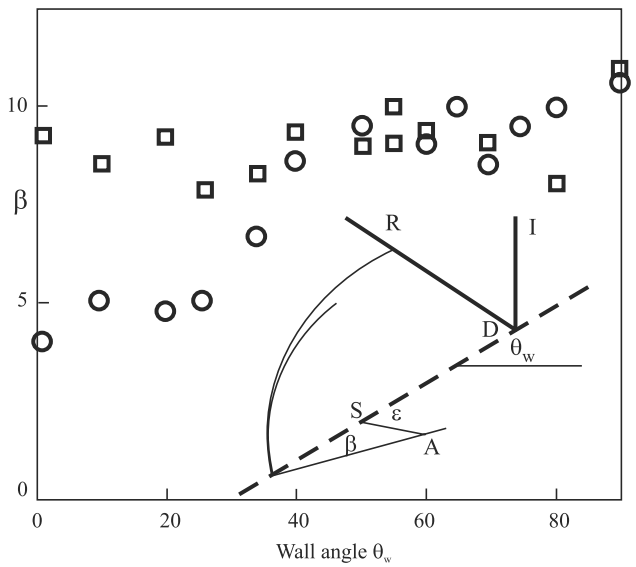

Fig. 7 Wall inflow angle. *Squares* from oblique shock analysis, *circles* from perturbation analysis

5 Wall reflection

Very instructive results may be obtained from the study of the wavelets generated from the reflection of a shock wave from a curved surface. Figure 8 shows two images taken 40 μs apart using a high framing rate digital camera. The first shows a Mach reflection off the shallower part of the surface and the second a transitioned regular reflection (Ben-Dor 2007). These are the two forms of reflection currently documented and accepted for shock reflection off a circular arc.

For the purpose of the current discussion two issues are of significance. Although the leading edge of the circular arc model is sharp, it still causes a sufficient disturbance to generate a very weak corner signal (C) which is just discernable in the images of Fig. 8. This is very important as it delineates the boundary between the flows that are influenced by the presence of the surface from the uniform flow that is outside its region of influence and which has been induced behind the incident wave.

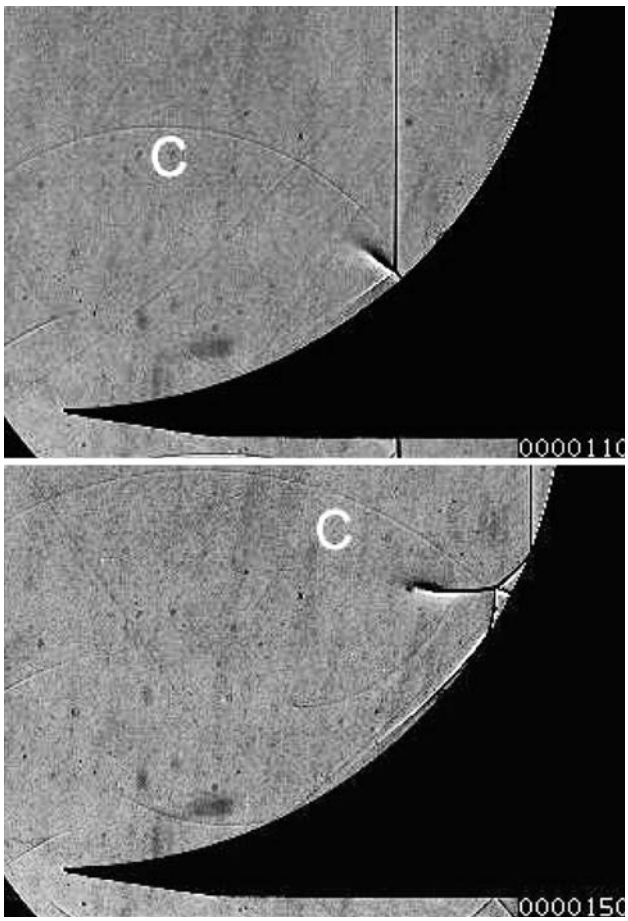

Fig. 8 Shadowgraph images of shock wave reflection from a circular arc surface. Incident shock Mach number M_s = 1.24. C is the weak corner signal arising from the inlet

The second issue is that the reflected wave in all images appears to broaden out and then terminate in space so that the cause and the structure of its development are not apparent. The issue arises that if a sufficient number of these perturbations were visible a much clearer understanding of the flow would be available. This conclusion is central to what follows. An ideal manner in which to study the temporal growth of the various features is by time-resolved photography where the propagation of individual wavelets may be monitored as they propagate outwards from the wall. Highly sensitive shadowgraph and schlieren imaging techniques are required to resolve the wavelets which need to be arranged to be weak so that they travel close to the local sound speed.

In a current study the perturbation sources are positioned by placing transverse strips of 45 μm thick tape onto the wall. In the case of strong waves it is found that natural wall roughness can also act as a suitable source even though the surface has been smoothed to remove machining marks. A Shimadzu HPV-1 high-speed digital camera was used to obtain the video clips. Framing rates were varied between 125 kfps and 1 Mfps (fps = frames per second) with exposure times per frame of between 250 ns and 1 μs. 102 frames are obtained in each test. The obtained image sequences can be played back as video clips which then give an excellent understanding of the evolution of the flow. Selected frames from some of these tests are given below. The benefits of high-speed time-resolved imaging of this sort are very significant and enable much improved physical insight into the flow processes. The ability to identify the propagation of a specific perturbation, during the playback of the movie, right from where it is initiated on the wall and throughout the flow field enables conclusions to be drawn as to which part of the flow is influenced from which portion on the wall, as well as which regions of the flow have not received any information from a particular point on the wall, and are therefore unaware of those changes in wall shape.

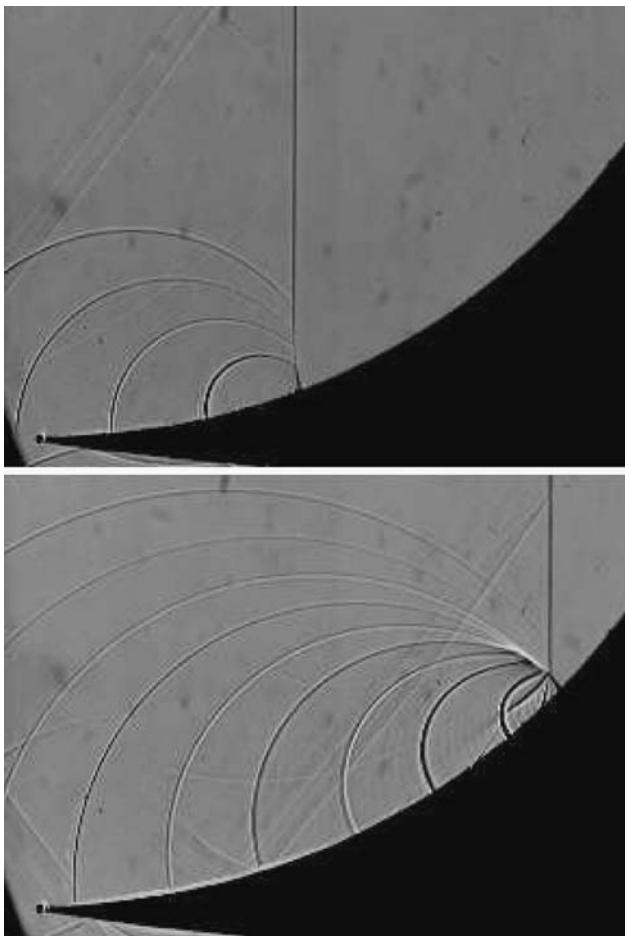

Fig. 9 Reflection off a circular arc of larger diameter than in Fig. 8 with perturbation sources on the wall. $M_s = 1.33$

5.1 Concave walls

Figure 9 shows two frames from a single test at times of 100 and 200 μs from when the shock meets the model inlet tip. A significant amount of additional information becomes available with the inclusion of the perturbations compared to that in Fig. 8.

Firstly, even at the time of the first picture when the incident wave has well advanced up the slope, a Mach reflection has not yet formed, in contrast to what is suggested in the literature (Ben-Dor 2007). There the triple point trajectory is sketched as if it exists from the start of the interaction, although the early parts of the trajectory are shown dotted because of lack of data. In Fig. 9 the perturbations are seen to spread out in a compression wave causing the shock to bend smoothly forward, the shape of the shock being influenced by the proximity of the successive compression waves. A Mach reflection with a distinct kink in the shock contour only develops when the disturbance waves begin to coalesce in a single point on the incident wave. Secondly, once Mach reflection has occurred, as shown in the second image, the corner signal from the model lip as well as the disturbance waves generated by the first tapes on the model meet the incident shock above the triple point. Hence they do not form part of the reflected wave as occurs for perturbations that are caused by the tapes located further up the slope. The reflected wave is thus generated from compression waves generated by only a portion of the arc. It also means that the incident wave is not of constant strength right down to where it meets the reflected wave so that the application of standard three-shock theory becomes inexact, although it is frequently assumed in the literature to be applicable. Wavelets coming from elements of wall roughness also become

evident as the Mach stem strength increases. These issues are discussed more fully in (Skews et al. 2008).

5.2 Convex walls

The case of a planar shock wave impacting on a circular cylinder is well documented, see, e.g., the summary given by Ben-Dor (2007). The ensuing reflection pattern typically undergoes some significant changes during the passage of the wave over the cylinder. For an initial wall angle of 90°, the reflection at the onset of the interaction is always regular, that is, the wave system consists of the incident wave and the reflected wave as shown in Fig. 10a. While the wave continues to travel up the convex surface of the cylinder, the wall angle decreases and thus the reflection conditions continuously change (hence this is a truly non-stationary reflection process). At some wall angle Θ_{trans} a regular reflection pattern can no longer be maintained and the reflection becomes irregular. This transition is marked by the appearance of additional waves and discontinuities. The wall angle of transition, Θ_{trans}, depends on the incident shock Mach number, the initial wall angle (in the case of partial cylindrical obstacles), the cylinder radius, and on the surface roughness (Ben-Dor 2007). Depending on the initial conditions, other types of irregular reflection may develop further downstream. The case most extensively studied is the transition from regular to Mach reflection, which is the only possible transition for weak shock waves ($M_S < 1.4$). The typical wave pattern, consisting of incident and reflected wave, a Mach stem and a contact surface, is shown in Fig. 10b. All experimentally recorded transition angles lie considerably below the corresponding values for the pseudo-stationary reference case of shocks passing over straight wedges. This means that during the interaction with the cylinder, a regular reflection pattern is maintained up to wall angles at which the pattern would already have transitioned into Mach reflection in the case of straight wedges. A convex surface therefore appears to be capable of delaying a transition compared to a straight one.

For the pseudo-stationary reflection over a straight wedge, one of the accepted and experimentally proven transition criteria is the so-called sonic criterion (Ben-Dor 2007). As long as disturbances generated behind the reflection point cannot catch up with it, the reflection remains regular. This is equivalent to the flow behind the reflection point travelling at supersonic speed in a frame of reference attached to the reflection point. As soon as this flow speed drops to sonic velocity, disturbances begin to catch up and the resulting reflection pattern becomes irregular.

The described perturbation technique was used to experimentally determine whether an analogous criterion also exists in the fully unsteady shock interaction with a cylinder. In the tests, the model was a cylinder of 150 mm diameter

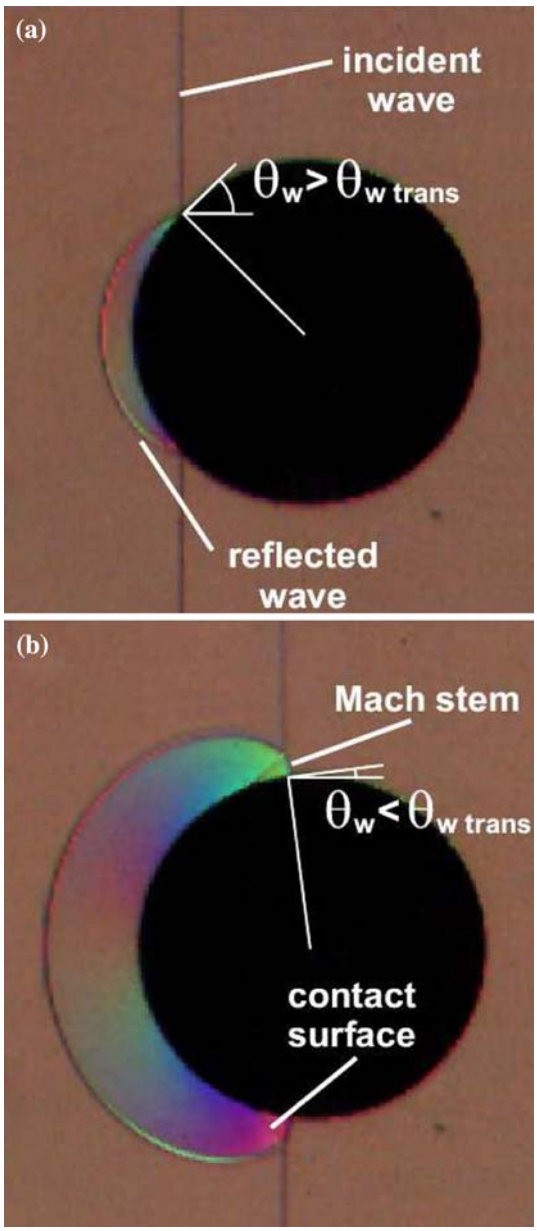

Fig. 10 Two images of the interaction of a planar shock wave with a cylinder; interval between images: 18 μs; shock Mach number M_s = 1.36; cylinder diameter: 30 mm

that was subjected to shock waves with shock Mach numbers between 1.2 and 1.35 in air. The interaction process was visualized with the schlieren system/high-speed digital video camera combination described at the beginning of this section. After reference tests with a smooth cylinder surface, tapes of 6 mm width and 70 μm thickness were applied at equal intervals. This way, a weak disturbance signal was created every 6 mm along the cylinder surface.

From the brief description given above it follows that the temporal development of each of these perturbations will differ depending on the nature of the reflection. In the

regular reflection regime, the disturbance signal is "shed" and left behind in the flow following the reflection point, while in the irregular reflection regime, it remains attached to the reflection point, similar to the configuration sketched in Fig. 3. The disturbance signal therefore has a forward and a rearward facing front as long as the flow behind the reflection point is supersonic, while its forward facing front merges with the reflected wave and the Mach stem as soon as the signals can catch up with the reflection point. Once this position on the cylinder is reached, only rearward facing disturbance waves are generated.

Through a time-resolved observation of the evolution of the pattern one can then determine which edge of the tape causes the last disturbance wave that is still left behind. In between this disturbance source and the next, the flow reaches sonic speed with respect to the reflection point. Upstream of this position, only regular reflection is possible, while irregular reflection can potentially develop once sonic flow speed has been reached in the region behind the reflected shock—provided the sonic criterion is also valid for curved surfaces.

The evaluation of the obtained visualizations showed that a visible Mach stem develops at wall angles that agree very well with the measurements summarized in (Ben-Dor 2007), both for a smooth and a taped model. Figure 11a shows the flow field about 20 μs after the Mach stem has first become visible. The point of sonic flow velocity, on the other hand, was reached considerably earlier in the process, typically at wall angles ten degrees higher than the angles at which the irregular pattern became visible. Figure 11b shows that only seven forward facing waves are trailing the reflection point, although at this point the wave has passed over fourteen disturbance sources. By contrast, the number of rearward facing waves caused by the disturbances matches the number of steps introduced by the tape (in Fig. 11b, three of these waves have already left the field of view). Although it is possible to arrive at similar conclusions with only a single image such as Fig. 11b, time-resolved visualization is highly beneficial to clarify the generation process of the waves produced by the disturbance sources and to remove possible doubts concerning the origin and the development of the disturbance waves. The findings regarding the point at which sonic velocity is reached may have significant consequences for the interpretation of reflection processes over curved surfaces, and particularly for the point at which the Mach stem actually erupts from the surface. Because of the large difference between the angle at which the Mach stem becomes visible and where the flow behind the reflection point becomes sonic, further investigations are required to fully clarify this issue.

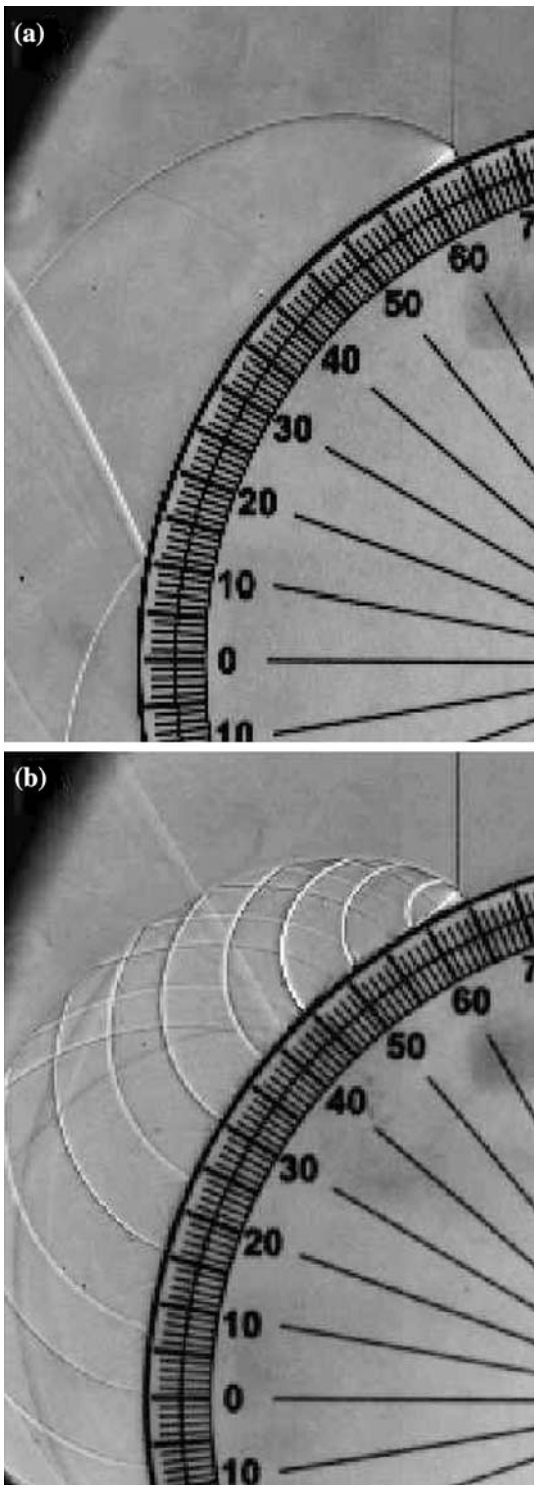

Fig. 11 Single frames from two time-resolved visualizations of the interaction of a planar shock wave ($M_S = 1.23$) with a cylinder (diameter 150 mm); front-lit omnidirectional schlieren images obtained at 250,000 fps. **a** Smooth cylinder; flow field at approximately 20 μs after Mach stem can be discerned on the image. **b** Taped cylinder (evenly spaced 6 mm wide tape); same instant as in (**a**)

6 Shock wave focusing

A particularly valuable aspect of this perturbation tracking technique is in the study of shock wave focussing since the influence of each change in wall direction can be followed throughout the flow. The focusing in a cylindrical cavity using time-resolved imaging is described in (Skews and Kleine 2007). The online version of this paper contains movies utilising this technique. The gas dynamic focus is defined as the location where the converging curved wave reflected off the back wall reduces to a point and the shear layers from either side of the cavity meet on the plane of symmetry. A comparison between a very weak shock wave focusing in a cylindrical cavity and that in a parabolic cavity of the same depth-to-aperture ratio is given in Fig. 12. The contrast in these images has been enhanced to make the perturbations more visible since they are even much weaker than the incident wave of $M_s = 1.03$. This image illustrates the exceptionally high sensitivity that can be achieved.

In the cylindrical case, the first perturbation, which arises from the entrance lip of the cavity, is stronger than the other perturbations because of the bluntness of the inlet edge. It completely overruns the focal point at the time of focus and so do the second and third perturbations. It is only the later perturbations which converge on the focal point thereby indicating very clearly that it is only the inner portion of a cylindrical reflector which gives rise to high focal pressures. The situation is somewhat different for the parabolic cavity. Here the first wave, called the lip shock, is much stronger than the perturbations produced by the tape because of the finite inlet angle of a parabolic cavity. Nevertheless all the waves tend to converge to a single focal point.

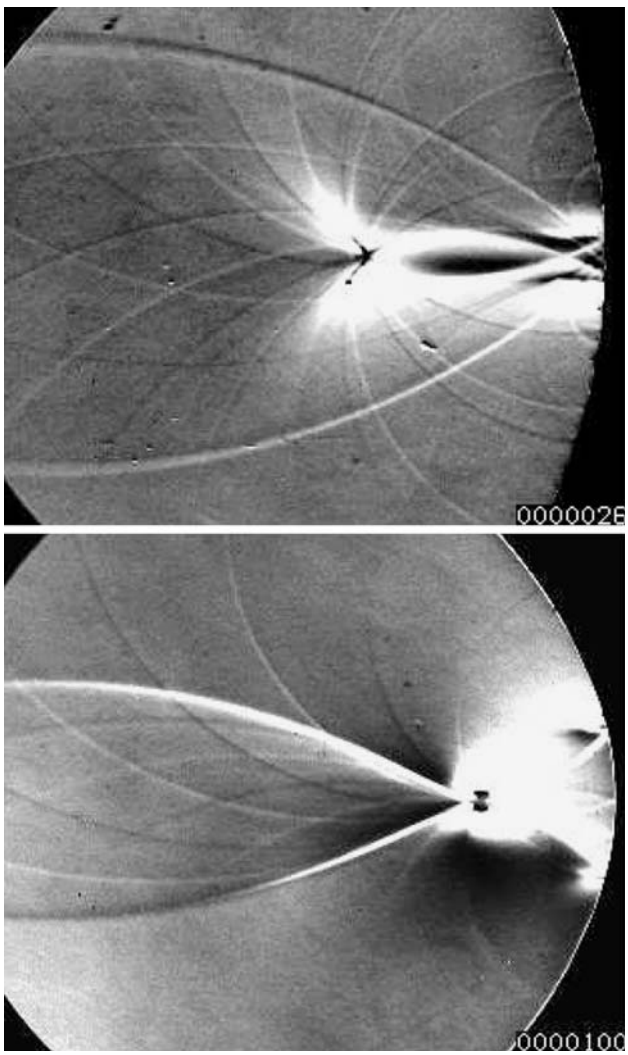

Fig. 12 Comparison of flow fields at the instant of gas dynamic focus for very weak ($M_s = 1.03$) shock waves in a cylindrical and a parabolic cavity

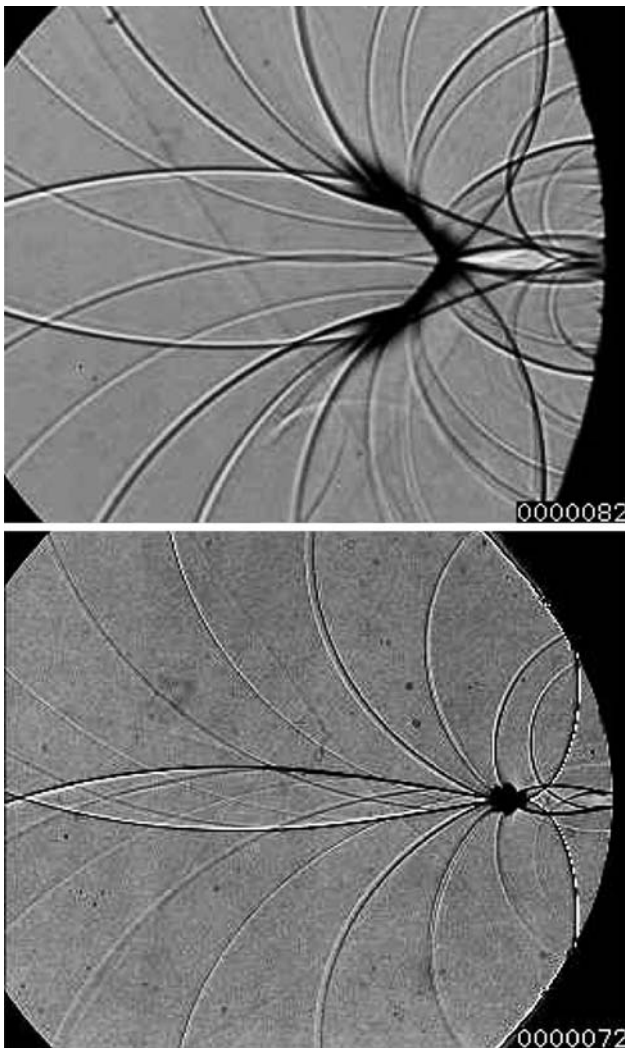

Fig. 13 Perturbation fields at focus for a cylinder (M_s = 1.23) and a parabola (M_s = 1.24)

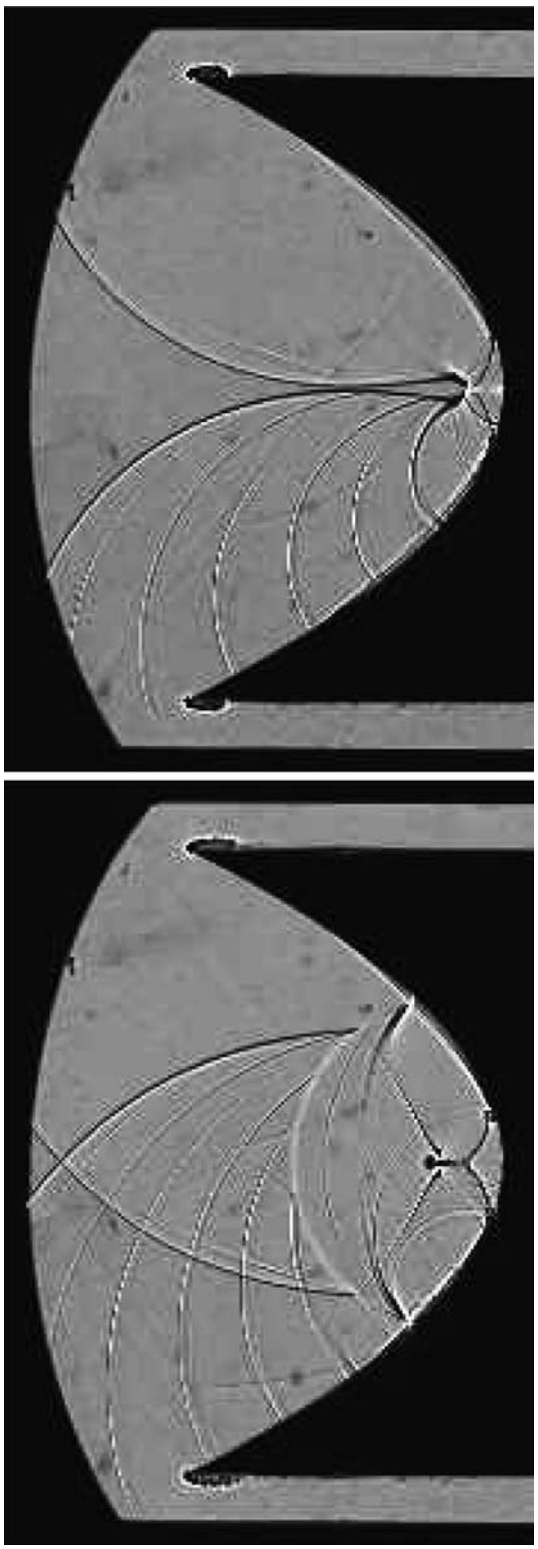

Fig. 14 Test on parabola with 47 μm tape positioned on one side only with steps at 12.5 mm pitch. $M_s = 1.34$, 80 μs between frames

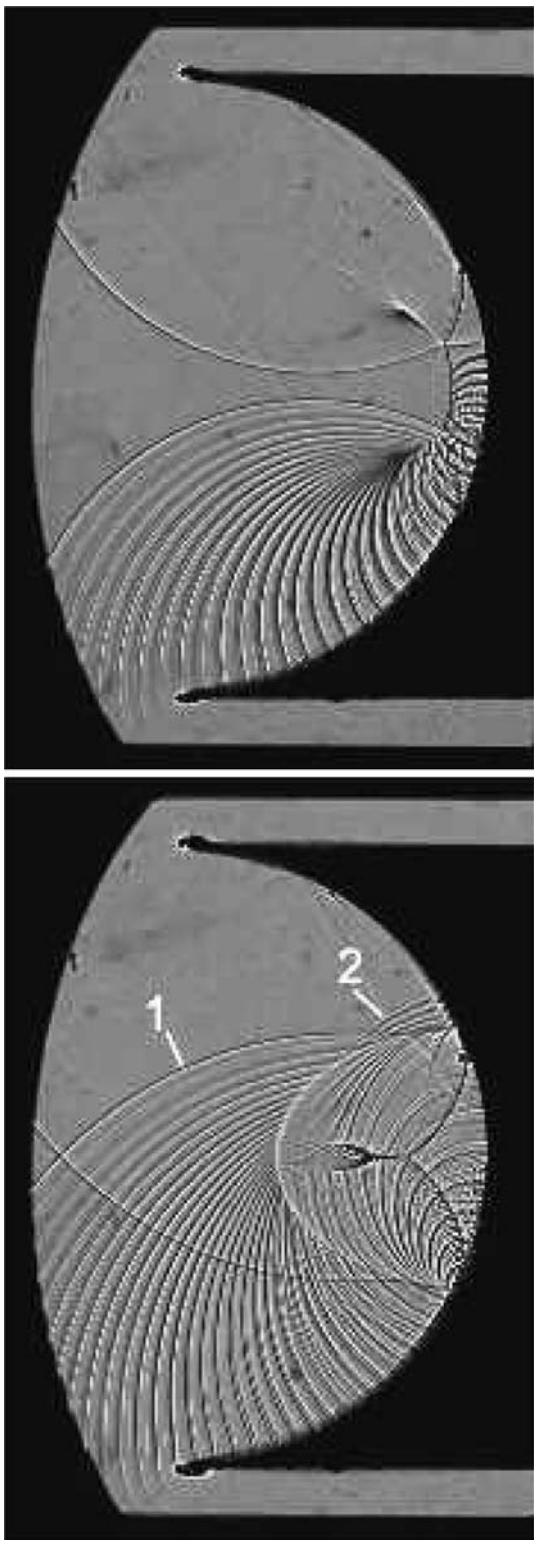

Fig. 15 Test on cylinder with 150 μm tape positioned on the lower side only with steps at 4 mm pitch. $M_s = 1.34$, 80 μs between frames

The effects of the non-linearity in shock reflection behavior is evident by repeating tests such as those above for stronger shocks. Figure 13 shows typical results. For the cylinder, the perturbations generated in the entrance region of the reflector still propagate beyond the focal point but the ones generated further downstream combine to

form the reflected wave, and it is the reflected shock waves from either side that meet at the focal point. For the parabola, the perturbations generated early in the focusing process meet on the lip shock rather than converging to the focus as seen in Fig. 12. If it were not for the presence of the lip shock they would bypass the focal point. The non-linearity of the focusing is graphically displayed by the distribution of the perturbations: the higher the shock Mach number, the more perturbations miss the focal point, which indicates that an increasingly smaller portion of the reflector contributes to the peak pressure in the focus. Equivalently, the spread of the perturbations is testimony to an enlargement of the focus area with an associated drop in peak pressure.

An interesting aspect of these images is the change in shading from one perturbation to the next. In general a perturbation showing up as a white/black line is followed by one appearing black/white. This is particularly prevalent for the perturbations produced in the early stage of the reflection, before the complicated Transitioned Regular Reflection pattern (Ben-Dor 2007) develops, when there are two closely spaced shocks propagating along the wall (see Fig. 8; Skews and Kleine 2007). The reason for this is that the tape, which is 12.5 mm wide, is placed with a gap between them of the same width. The shock passing over them thus first experiences a step up onto the surface of the tape resulting in a compression immediately followed by an expansion. These are closely coupled because of the tape being very thin. When the shock passes off the edge of the tape the reverse happens and there is initially a wave diffraction over the edge resulting in an expansion followed by a compression as it strikes the model surface.

An important issue to address is whether the presence of the tape, with its resultant series of steps, has any influence on the flow field, so that it can be used for diagnostic purposes without itself modifying the flow. Figure 14 shows two frames from a single test taken with a shock of $M_s = 1.34$ and the tape positioned only on the lower half of the cavity. A stronger shock is chosen for this test in view of the increase in expected dissipation. The first image is taken just before focus and the second 80 μs later.There is no discernable difference of the flow features between the upper and lower sides of the cavity, and the features are completely symmetrical. It is interesting to note how the perturbations terminate on the lip shock in the early image and on the main reflected shock on the later one. The difference is that the waves arise behind the shock in the first and catch up with it, and that they are overtaken by the main reflected shock in the second. This is simply in accordance with a disturbance propagation on either side of a shock, since the flow relative to the shock is supersonic on one side and subsonic on the other.

In order to apply a more severe test, the cylindrical cavity was fitted with much thicker tape, of 150 μm thickness and 1 mm width, positioned at a pitch of 4 mm on the lower surface. These results are shown in Fig. 15 for the same shock Mach number and frame interval as Fig. 14. In this case, although the wave patterns remain symmetrical, the shear layer resulting from the initial Mach reflection on the lower wall appears to have been somewhat disrupted, probably resulting from its very close proximity to the tape. What is very interesting, however, is that the envelope surrounding the perturbations contains two distinct wave fronts, one being the corner signal (lip shock) and the other coming from behind the focusing reflected wave. These are denoted 1 and 2 on the figure. Thus the influence of the lower wall does not only propagate in cylindrical fashion behind the corner signal from the cavity lip, but accelerates behind the focussing shock to emerge ahead of the lip perturbation. This influence would not become apparent in tests without the disturbances since these fronts are moving into non-uniform, smoothly varying flow fields generated by the opposite surface. Thus the existence of the wave front 2 from that generated from the upper wall is not evident in the flow in the lower half of the cavity. These wave fronts are also unlikely to be identified from numerical simulations containing small perturbation sources on the walls, unless the resolution is sufficient to capture, not only the shocks, but these very weak waves as well, since they may be similar in magnitude to numerical noise.

7 Conclusions

A diagnostic method is described for the study of flows induced by shock waves, which shows in a graphical way how information passes from one point of a flow field to another. Further developments of the technique will be to extract quantitative information, such as velocity and temperature, from the motion of the perturbations. Time-resolved imaging, without having to account for issues of reproducibility inherent in single-shot testing, makes this a viable and attractive possibility to determine the mechanisms responsible for the generation of certain flow patterns.

References

Ben-Dor G (2007) Shock wave reflection phenomena. 2nd edn. Springer, Heidelberg

Lilley GM, Yates AH (1953) Some aspects of noise from supersonic aircraft. J Roy Aero Soc 57:396–414

Lock GD, Dewey JM (1989) An experimental investigation of the sonic criterion for transition from regular to Mach reflection of weak shock waves. Exp Fluids 7:289–292

Seitz MW, Skews BW (2006) Effect of compressible foam properties on pressure amplification during shock wave impact. Shock Waves 15:177–197

Skews BW (1967) The shape of a diffracting shock wave. J Fluid Mech 29:297–304

Skews BW (2005) Shock wave interaction with porous plates. Exp Fluids 39:875–884

Skews BW, Kleine H (2007) Flow features resulting from shock wave impact on a cylindrical cavity. J Fluid Mech 580:481–493

Skews BW, Takayama K (1996) Flow through a permeable surface due to shock wave impact. J Fluid Mech 314:27–52

Skews BW, Kleine H, Bode C, Gruber S (2008) Shock wave reflection from curved surfaces. 22nd Int. Congress on Theoretical and Applied Mechanics, Adelaide, Australia

Whitham GB (1967) A new approach to problems of shock dynamics. Part 1. Two-dimensional problems. J Fluid Mech 2:l45–171